Joint Power, Frequency and Precoding Optimisation in a Satellite SDMA Communication System

Joint Power, Frequency and Precoding Optimisation in a Satellite SDMA Communication System

Florian Vidal
Direction of Research
Thales Alenia Space
florian.vidal@thalesaleniaspace.com

Hervé Legay
Direction of Research
Thales Alenia Space
herve.legay@thalesaleniaspace.com

George Goussetis
Institute of Sensors, Signals & Systems
Heriot-Watt University
Edinburgh, UK
G.Goussetis@hw.ac.u

***Abstract*—State-of-the-art satellite processors include the capacity to offer full digital beamforming. Digital beamforming used jointly with an active antenna allows a full power, frequency and beamforming flexibility. This flexibility must be utilised with efficient and fast computing resource allocation algorithms, especially in a MEO use-case. As MEO satellites move with respect to Earth contrary to GEO satellites, they experience very diverse user distributions and must dynamically adapt the resources allocated to each user. This paper proposes an algorithm based on SDMA which leverages the payload flexibility with a joint power, frequency and beamforming optimisation. The algorithm provides a fair resource allocation to users, accounting for their respective required spectral efficiency.**

Keywords— Digital beamforming, MEO, precoding, resource allocation, SDMA.

I. INTRODUCTION

Today satellite communications are driven by an increasing demand in data rate per user terminal (UT) with a diversification of services including broadband internet. This motivates the use for higher frequencies where more bandwidth is available. These mm-wave frequencies enable to form multiple narrow beams with an antenna that can be fitted on the satellite platform. Highly directive antennas enable a frequency reuse scheme which increases the aggregated bandwidth exploited while limiting inter-beam interference [1]. The most common orbit for satellite communication is the geostationary one (GEO) which allows low-complexity UTs (no tracking of the satellite is needed) as well as a wide Earth coverage. GEO, however, suffers from latency issues with between 500-600 ms round-trip time latency. High latencies are particularly detrimental in the case of a satellite integration with 5G where applications such as UAV control or remote health monitoring are latency critical [2]. MEO appears as a relevant alternative with a fiber-like latency of around 130 ms [3]. O3b MEO constellation is currently operational with 20 satellites in orbit, each one generating 10 user beams by means of reconfigurable reflector antennas. This antenna configuration is limited in the number of users each satellite can serve. To keep the pace with the increasing number of customers, next generation O3b satellites will be able to generate 4,000 user beams by means of antenna arrays [4]. Guaranteeing a high quality of service for the 4,000 users would require a smart management of interference with frequency, power and spatial diversity. The following contribution proposes to tackle an intermediate use-case between O3b first generation and O3b mPower by considering 100 users.

Space division multiple access (SDMA) exploits the spatial diversity of users to send interference free data streams. It was first suggested in [5] to utilise array processing for reducing the interference between users who use the same frequency and time resource. This approach was proposed in [6] for an extension of 4G services by satellite. SDMA increases the frequency reuse factor by mitigating the interference, which is crucial when the frequency resource is scarce. Moreover, each user is centered in its own beam (Earth-fixed cell) [7] so the gains are higher than in a fixed coverage from the satellite perspective (satellite-fixed cell). In [6] a dynamic beamforming strategy optimises the radiation patterns toward each UT while a resource allocation algorithm allocates frequency bands in a way to avoid inter-beam interference. Algorithms to implement SDMA with frequency resource allocation were developed in [8]. They are based on a greedy algorithm that seeks to minimise the aggregated interference affecting each user and integer linear programming (ILP) approaches. Reference [9] adds a degree of freedom to manage interference by virtue of time resource. References [8-9], however, do not consider an optimum beamforming but only beams steered to user positions. Reference [10] proposes to add the ability to slightly steer the beams to reduce inter-beam interference. SDMA with more complex antenna processing for a satellite application was investigated in [11] and performed jointly with the greedy resource allocation algorithm presented in [8]. These past years, novel linear precoding schemes to mitigate inter-beam interference were proposed in the literature [12]. The following paper proposes a joint frequency, power and precoding optimisation applied to MEO satellites using Ka band. The presented approach can be extended to other orbits such as GEO. The objective is to maximize the number of users served with a minimum spectral efficiency. It is crucial as satellite operators commit a certain minimum data rate per UT. The forward link between the satellite and the user terminals is considered in this paper. In the first section, the satellite payload models and the channel model are described. Then, the second section presents a resource allocation algorithm that jointly optimises frequency, power and precoding. Finally, section three highlights the benefits of the joint optimisation with estimations of the numbers of users served.

II. SYSTEM MODEL AND CHANNEL MODEL

A. Antenna models

The choice of the satellite antenna depends on the targeted coverage and orbit. In the case of a limited coverage, for example focusing on Europe, reflector antennas may be privileged [6]. If the objective is to cover all the visible Earth from the satellite point of view, a direct radiating array (DRA) is more adapted [11]. In MEO, as the field of view of the satellite is large (about 20°) and a full flexibility to steer the antenna beams is required, a DRA is preferred. The antenna presented in Fig.1 was identified as a promising DRA candidate for MEO applications when used jointly with precoding [13]. There are three different radiating tiles made of square elementary radiating elements of size 1.2λ. The positions of the tiles of this sparse array

This work was supported by the European Commission under H2020 project REVOLVE (MSCA-ITN-2016-722840)

antenna follow the pattern of a sunflower [14], it has several advantages:

- Low first side-lobe levels due to a spatial tapering of the radiating elements following a Taylor amplitude distribution.
- The sunflower design requires a reduced number of radiating elements compared to conventional array antennas . Reference [13] shows a reduction of 40% in the number of radiating elements compared to a conventional circular array. This results in a reduced number of RF chains and payload hardware complexity. A RF chain consists in a cascade of RF components such as ADC, DAC, high power amplifiers, frequency mixers.
- The spacing between the tiles produces a larger antenna diameter without increasing the number of radiating elements compared to a conventional array. Consequently a narrower beamwidth is achieved, which is beneficial when it comes to form nulls in the radiation pattern of the antenna. The less correlated channels between beams and users explains these improvements. The 3 dB beamwidth of the antenna considered in this paper is 1.6°.
- No grating lobe, this is due to the irregular layout of the tiles.

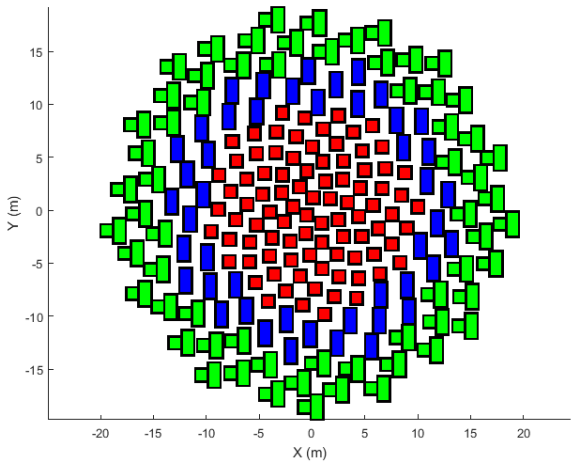

Fig. 1. Radiating elements layout for the sunflower antenna with three different tiles composed of one (in red), two (in blue) or three (in green) elementary radiating elements.

The larger tiles are positioned on the outer of the array to fill the space between the radiating elements (as the density of tiles is reduced at the edge of the array) and increase the aperture efficiency.

The inconvenients of this antenna are the manufacturing because of the non-uniformity of the layout, high side lobe levels and high scan losses which implies different amplitude signals for each UT. These last two impairments are illustrated in Fig. 2 which represents the radiation patterns of the sunflower antenna at boreside and when scanning the beams at the edge of coverage.

To tackle these issues, the high scan losses can be alleviated with precoding techniques and non-uniform attenuations by power control. The complete benchmark with a conventional circular DRA was made in [13]. In the following, the link budget computations are based on the radiation patterns of the sunflower antenna presented in Fig. 2.

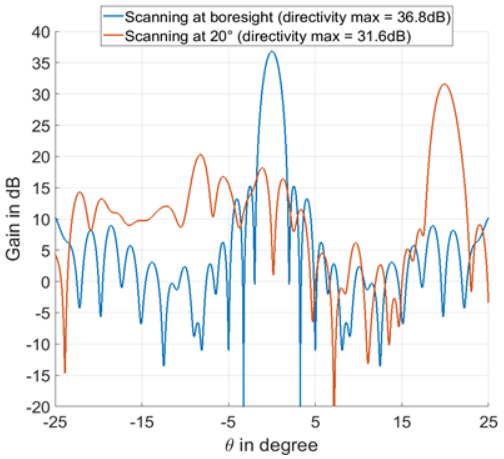

Fig. 2. Radiation pattern of the sunflower antenna at boreside and when scanning at the edge of the coverage.

B. Channel model

The data rate that can be achieved with a given bit error rate depends on the channel state between the satellite and the UTs. The channel is supposed to be line-of-sight (LoS) with no blockage and one beam formed per user in a SDMA scheme. The channel matrix is denoted $\mathbf{H} \in \mathbb{C}^{K\times K}$, with K the number of user antenna beams, which is the same as the number of users. Each entry $h_{i,j}$ of matrix $\mathbf{H}$ models the channel between beam j and user i and is defined in (1).

$$h_{i,j} = \sqrt{G_{i,j} L_{FSL_i} L_{atm_i} \left(\frac{G_{UT}}{T}\right)_i \frac{1}{kB_j}} \tag{1}$$

Where $G_{i,j}$ is the gain of beam j toward user i. When $i = j$ the useful signal is considered, otherwise the matrix entry refers to the amplitude of an interfering signal. In this study we considered real numbers entries for the channel matrix. The phase excitation at each radiating element level is implicitly accounted in the gain of the total array which is deduced from phase laws designed to steer the beams at UTs' positions. Attenuation due to the free space path loss (FSL) and atmospheric absorption must be accounted for. In the scenario considered, clear sky is assumed meaning that only the free space losses are considered. Free space loss L_{FSL} is due to the attenuation of the electromagnetic waves in free space as they spherically spread whilst they propagate. The expression of FSL for user i is given in (2).

$$L_{FSL_i} = \left(\frac{4\pi d_i}{\lambda}\right)^{-2} \tag{2}$$

where λ is the wavelength of the carrier signal and d_i is the distance between the satellite and the user i. Finally, the gain and noise of each UT is captured in the figure of merit G_{UT}/T with G_{UT} the gain user terminal antenna and T the noise at the receiver. This noise takes into account atmospheric and receiver signal chain noise.

The signal received at the user terminal *i* can be modeled as:

$$\mathbf{y} = \mathbf{HWx} + \mathbf{n}$$

where $\mathbf{y} \in \mathbb{C}^{K\times 1}$ is the signal received by each user from *K* beams; **W** is the precoding matrix with $\mathbf{W} \in \mathbb{C}^{K\times N}$; *N* is the number of antenna feeds; $\mathbf{x} \in \mathbb{C}^{N\times 1}$ contains the complex transmitted symbols at each antenna feed $n \in [1, N]$; and the vector $\mathbf{n} \in \mathbb{C}^{K\times 1}$ represents the independent and identically distributed zero mean and unit variance Gaussian noise.

An upper bound for the capacity achieved by a satellite payload is given by the sum-rate of the system [15]. This is defined as:

$$\mathrm{SR} = \sum_{i=1}^{K} \log_2(1 + \mathrm{SINR}^{[i]})$$

In (4), $\mathrm{SINR}^{[i]}$ is the signal over noise plus interference ratio experienced by user *i*. The SINR is defined as:

$$\mathrm{SINR}^{[i]} = \frac{1}{\left((\mathrm{C/N})^{[i]}\right)^{-1} + \left((\mathrm{C/I}_{interbeam})^{[i]}\right)^{-1} + \left(C/I_{intermod}\right)^{-1}} \quad (5)$$

Where the expression of the carrier over noise is:

$$(\mathrm{C/N})^{[i]} = p_i|\mathbf{h_i}\mathbf{w_i}|^2$$

In (6), $\mathbf{w_i}$ the i^{th} column of the precoding matrix **W**, $\mathbf{h_i}$ the i^{th} row of the channel matrix **H**, and p_i the power of the carrier allocated to user *i*. The sum of the p_i must be less than the total power available on-board *P* and are determined with a smart power allocation algorithm described later in section III.B. If user *i* is allocated carrier frequency *n*, the carrier over interference power ratio can be expressed as:

$$(\mathrm{C/I}_{interbeam})^{[i]} = \frac{p_i|\mathbf{h_i}\mathbf{w_i}|^2}{\sum_{j\neq i}^{K} f_{j,n} p_j \left|\mathbf{h_i}\mathbf{w_j}\right|^2}$$

The frequency carriers to beams allocations are stored in a binary matrix $\mathbf{F} \in \mathbb{N}^{K\times N_f}$ where N_f is the number of available frequency carriers. Each element of the matrix **F**, $f_{i,n}$ indicates if the beam *i* is allocated to the frequency chunk *n* if $f_{i,n} = 1$, 0 otherwise. **F** is the matrix which is optimised by the frequency resource allocation algorithm presented in section III.A. Beams can interfere only if they share the same frequency carrier.

As the antennas are required to operate in multicarrier mode, intermodulation interference caused by the non-linearity of amplifiers must be taken into account. Values for Solid State Power Amplifiers (SSPAs), depending on the power amplifiers operating points, are given in [16]. Given [16] and a 3 dB output back-off (OBO), a carrier-to-intermodulation ratio of 17 dB is assumed. In the scenarios further considered, even if this parameter plays a role in the link budget, the inter-beam interference remains the major limiting factor of SINR in most cases.

Based on the users' SINR values, a spectral efficiency expressed in bps/Hz can be derived from the DVB-S2 standard [17]. To reach an objective spectral efficiency a threshold SINR value is required. The following sections show how precoding and resource allocation are key enablers to reach this threshold.

C. Precoding scheme

The precoding matrices can be computed on-board or on-ground. The former would reduce the time before the precoding matrix is updated since no support from the gateway is required. The satellite processor complexity, however, is increased and [13] suggests that a dedicated processor would be needed to operate on-board precoding. The latter solution is to generate the precoding matrices at gateway level. This would reduce the on-board processor complexity but increase the time delay before acquiring the precoding matrix. It may be detrimental in the case of a MEO satellite moving dynamically with respect to Earth. The problem of whether on-board or on-ground precoding should be chosen is not addressed in this paper and it is only assumed that a precoding scheme is implemented in the system to mitigate interference in the forward link. Moreover, to reduce the dependency on the quality of channel state information (which may be challenging to collect for hundreds of users), it is assumed that the precoding matrices are computed only with the knowledge of UTs' positions and stored radiation patterns at gateway level. This way, an estimation of the channel matrix can be deduced. This approach is valid only in a LoS condition which is likely to be the case as O3b MEO constellation aims at customers such as cruise, aero, offshore and remote mining [18].

W is computed at beam level. It assumes a preliminary beamforming stage based on phase only weights is applied to maximise the power toward each user by summing coherently the signals at the output of each radiating element. In LoS, this beamforming strategy outperforms conjugate beamforming [19]. The resulting antenna gain is accounted in the channel matrix in (1) as $\mathrm{G_{i,j}}$. A minimum mean square error (MMSE) precoding is applied at beam level to cancel inter-beam interference due to the preliminary maximum gain strategy. This precoding at beam level has the advantage of processing simpler $K \times K$ precoding matrices compared to $N \times N$ feed level precoding matrices (with $N > K$). The MMSE matrix is obtained through (15) and is normalized according to the CTTC approach described in [20] which proved to perform the best compared to other existing normalization strategies. A precoding matrix normalisation is adopted so the focus on power optimisation is made in a different step of the optimisation process later discussed in section III.B.

$$\mathbf{W}_{\mathrm{MMSE\ not-normalized}} = (\mathbf{H}^H\mathbf{H} + \delta\mathbf{I}_N)^{-1}\mathbf{H}^H \quad (15)$$

The coefficient δ is used for regularisation, it is fixed and defined with a heuristic that optimises the sum rate on uniform scenarios of user distribution:

$$\delta = 2 \times K \times \|\mathbf{H}\|_\infty$$

with $\|\mathbf{H}\|_\infty$ being the sup norm, which is the highest norm of **H** entries.

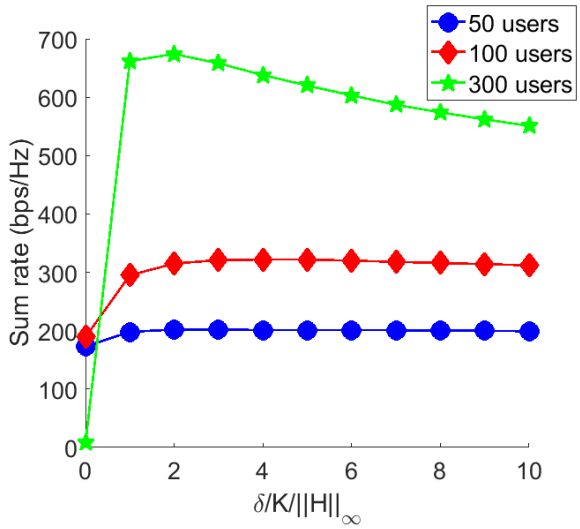

Fig. 3. Impact of regularisation on the sum rates achieved

The choice of the δ parameter was done by observing the sum rates achieved with a varying number of users and a varying regularization coefficient as presented in Fig. 3. The scenario considered in Fig. 3 focuses on uniform UTs distributions. A significant gain in sum rate is observed by increasing the regularisation parameter until an optimum value of $\delta = 2 \times K \times \|\mathbf{H}\|_\infty$. The sum rate gain achieved with regularisation rises with the number of users. Further increasing the regularisation parameter does not result in higher sum rates and even reduce the capacity in the case of 300 users.

The parameter found proved to also increase the sum rate on non-uniform user distributions [13].

III. Resource Allocation Algorithm

In the following sub-sections, the different domain of resource allocation are tackled. The optimisation is said to be joint as for each iteration of simulated annealing (SA), the precoding matrix and power allocation are adapted to account for the new candidate frequency plan.

A. *Frequency chunk allocation*

A resource allocation algorithm is used to optimise the number of users allocated with an objective SE. The algorithm is able to utilise the flexibility of the payloads accounting for MMSE precoding, power flexibility and an optimised allocation of frequency carriers. This algorithm is based on SA, which combines a global research and a local research in the set of feasible solutions following the flow graph in Fig. 4. SA was used in the literature to solve similar resource allocation problems in the context of satellite communication involving flexible resource allocation [21]. The candidate frequency plans are modeled by the **F** matrix previously introduced in section II.B. Only configurations with one carrier per beam are investigated. At each iteration of SA, a configuration is considered which evolves with iterations. Firstly, the algorithm explores the feasible domain of frequency allocations by allowing a wide set of configurations. As the temperature T decreases at each iteration as $T = \alpha T$, with α the cooling factor, lower than 1, this set becomes more restricted as the algorithm accepts only configurations that improve the number of users allocated or configurations with lower sum rate with a probability $exp(-(nbUsersAllocated_{old} - nbUsersAllocated_{new})/T$. Finally, as the selection of new configurations becomes more elitist, the algorithm can be seen as a local research where only the allocation configurations that improve the achieved number of users allocated are chosen. Improvements in the number of users allocated are achieved by removing interfering beams and allocating frequency carriers to beams that do not interfere with active neighbour beams.

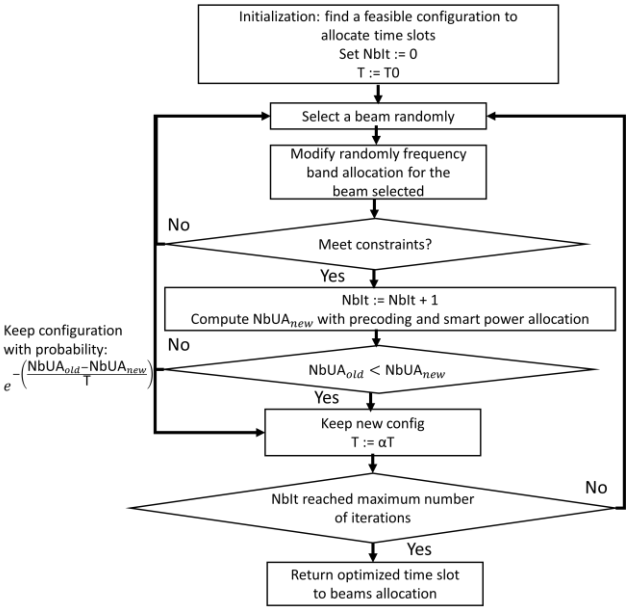

Fig. 4. Simulated annealing algorithm to allocate frequency bands/time slots to beams. NbUA = Number of users allocated the objective spectral efficiency.

An appropriate starting point frequency plan needs to be chosen to increase the quality of the optimum found with SA. This optimum may correspond to a greedy solution with for example the algorithm presented in [8]. The greedy algorithm, inspired from DSATUR graph colouring method, aims at minimising the aggregated interference experienced by each user at each frequency allocation.

An accelerated version of SA consists in a local approach based on hill climbing (HC). In this case the exploration step is skipped and only solutions which improves the number of users allocated are accepted. The running time is reduced with the risk to fall in a local optimum. SA is the algorithm showing the best results in terms of users allocated so it is the one used to obtain the results in section IV.

B. *Smart power allocation*

Applying the previous algorithm with a uniform power allocation for all carriers is insufficient to reach an objective spectral efficiency as UTs experience heterogeneous C/N. Worst path and scan losses at high beam steering angles harm UTs' power received. A method to efficiently allocate power to each user is proposed in [22]. The problem studied in [22] aims at minimising the total power required to meet the SINR constraints for each user. Given a precoding strategy l, the minimum power requirement for each user is given by (16).

$$\mathbf{p}^{min,l} = [\mathrm{diag}(\mathbf{\Psi}^l) - \mathbf{\Gamma}(\mathbf{\Psi}^l - \mathrm{diag}(\mathbf{\Psi}^l))]^{-1}\mathbf{\Gamma 1} \quad (16)$$

Where $\mathbf{1}$ is the unitary vector of dimension $\mathbb{N}^{K\times 1}$, $\mathbf{\Gamma}$ the diagonal matrix of size $\mathbb{R}^{K\times K}$ with on each element of the diagonal the objective SINR, γ_i, $i \in [1, K]$. $\mathbf{\Psi}^l$ is the coupling matrix obtained with precoding technique l, which describes the interference between users after applying precoding. Its expression is given in (17).

$$\mathbf{\Psi}^l = \begin{bmatrix} (\mathbf{h_1 w_1})^H(\mathbf{h_1 w_1}) & \cdots & (\mathbf{h_1 w_K})^H(\mathbf{h_1 w_K}) \\ \vdots & \ddots & \vdots \\ (\mathbf{h_K w_i})^H(\mathbf{h_K w_1}) & \cdots & (\mathbf{h_K w_K})^H(\mathbf{h_K w_K}) \end{bmatrix} \quad (17)$$

Reference [22] demonstrated that if all the entries of $\mathbf{p}^{min,l}$ are greater than zero, then a solution to the power minimisation problem with SINR constraints exists and is given in (16). Otherwise it means either that there is not enough power available (C/N too weak to reach the objective SINR), or that there is too much interference between users even with precoding (if users are co-located). The solution to obtain a feasible set of power levels is to allocate different frequency bands to the users with the algorithm presented in section III.A. In the following the problem is not to minimize power but to optimise a power distribution between beams given a total available power so the vector $\mathbf{p}^{min,l}$ is normalised to P.

IV. Results

A. Joint resource allocation and beamforming

When applying SA, precoding and smart power allocation are performed at each iteration. To illustrate the benefits of the algorithm, a scenario with 100 users is considered (see Fig. 5). The user distribution is represented in the satellite point of view in the true view angle coordinates. The link budget assumptions are presented in Table I.

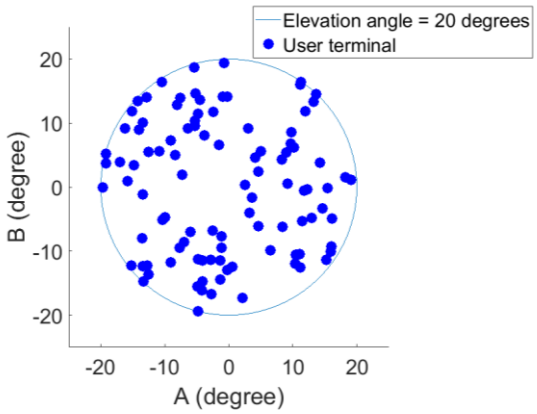

Fig. 5. Uniform UT distribution.

An objective minimum SE of 2.5 bps/Hz is targeted for all users. Consequently, the γ_i introduced in the power allocation scheme are the ones required by the DVB-S2X standard [23] to reach 2.5 bps/Hz. With 10 MHz carriers, this would guarantee each user to benefit from at least 25 Mbps. To illustrate the approach with a simple use-case, all the users are assumed to require a single carrier. However the SA algorithm developed can also provide a non-uniform resource allocation to beam as presented in [24]. Only two carriers are considered. This number is determined by how dense the user distributions are and the antenna beamwidth. If users are too close, they are required to use different carriers.

TABLE I
LINK BUDGET PARAMETERS

Central carrier frequency	20 GHz (Ka band)
Frequency bandwidth allocated to each user	10 MHz
Total RF power available	78 W
Satellite antenna gain at boreside	36.8 dB
Satellite antenna beamwidth	1.6°
User terminal gain over receiver noise G/T	21 dB/K (1.2 m UT)
OBO	3 dB

It was checked that the link budget parameters presented in Table I are compliant with ITU-R RR regulations [25] specifying a power spectral density of -115 dBW/m² for 1 MHz. Meeting this regulation is essential to exploit Ka band with non-geostationary satellites. The optimisation parameters of SA are presented in Table II.

TABLE II
SIMULATED ANNEALING PARAMETERS

Initial temperature	100
Decreasing temperature parameter α	0.98
Convergence criteria	100 iterations without improvement of NbUA

Table III and Table IV show the results and the benefits of a joint resource allocation respectively with one and two carriers. In Table III, with one carrier, full frequency reuse and no precoding, no user demand is met. When adding precoding 33% of the users benefit from the objective SE which is still not acceptable. High interference levels are due to many close users which interfere in this full frequency reuse scenario. The only solution is to extend the spectral resources with two carriers available at different frequencies with results presented in Table IV. The result of the frequency bands allocation is presented in Fig. 6. Close UTs are allocated carriers with different central frequencies. Without precoding still none of the demand is met. Precoding plus frequency allocation enable to increase the percentage of users allocated to 76% of the demand. By adding the smart power allocation, 100% of the demand is met. Fig. 7 shows that users at the edge of coverage are allocated more power. As explained before, this power adaptation compensates for the extra path and scan losses at high beam steering angles.

TABLE III
RESULTS RESOURCE ALLOCATION WITH ONE CARRIER

	Percentage users served (%)	Min. SE (bps/Hz)	Sum rate (bps/Hz)
Without precoding	0	0.39	148
Precoding	33	0.32	303

A significant power heterogeneity can be observed with power levels ranging from less than 0.4 W at the center of the coverage to 1.8 W at the edge of the coverage (6.5 dB difference). With 1.5 dB extra losses at the edge of coverage due to path losses at 8063 km and 5.2 dB antenna scan losses (see Fig. 2), the power compensation algorithm compensate the different attenuations experienced by the UTs in order to reach the minimum SE for all the terminals. An interesting fact is that in Table IV, the smart power allocation reduces the sum rate. As less power is allocated to UTs benefiting from "good" channels (with less losses) at the center of the coverage, the overall sum rate decreases. It highlights the conflicting objectives of optimizing the sum rate and having a fair resource allocation.

TABLE IV
RESULTS RESOURCE ALLOCATION WITH TWO CARRIERS

	Percentage users served (%)	Min. SE (bps/Hz)	Sum rate (bps/Hz)
Without Precoding	0	0.97	253
Without Precoding + smart power allocation	1	0.62	247
Precoding	76	2.0	412
Precoding + smart power allocation	100	2.7	398

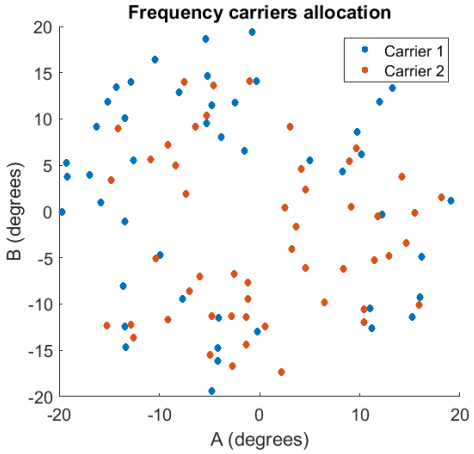

Fig 6. Frequency carriers allocation to reduce inter-beam interference.

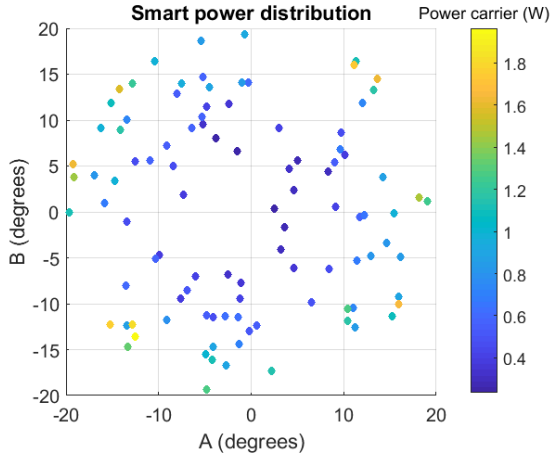

Fig. 7. Power allocated to each user.

B. *Benchmark of frequency allocation algorithms*

The frequency resource allocation approach presented can also be applied by substituting SA to the greedy algorithm presented in [8] or to a HC approach. For each number of users considered, 100 scenarios of user distributions were randomly drawn with users uniformly distributed. The number of users allocated the objective SE (in Fig. 8) and the running time (in Fig. 9) of the algorithms are averaged on the 100 runs.

As mentioned in [8] the greedy algorithm is almost instantaneous, however Fig. 8 shows also very poor results compared to SA with a number of allocated users dropping consequently after 20 users. Note that the results in [8] were obtained with eight different frequency bands whereas in this scenario only two frequency bands are allowed. Consequently SA is a more spectral efficient frequency allocation algorithms than the greedy approach. The efficiency of SA annealing comes at a higher computational cost as emphasized in Fig. 9 with lengthier calculations as the number of users increases, for example up to 60 s for 200 users.

HC offers a compromise between running time and performance. For 300 users, the running time is divided by three compared to SA for a reduction of 35% of the number of users allocated. As mentioned before it is due to a convergence toward a local optimum that SA is able to avoid.

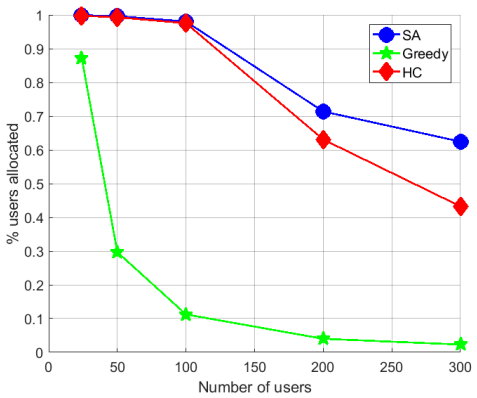

Fig. 8. Percentage of users allocated minimum SE: comparison SA/HC/greedy [8] algorithms with two frequency carriers available.

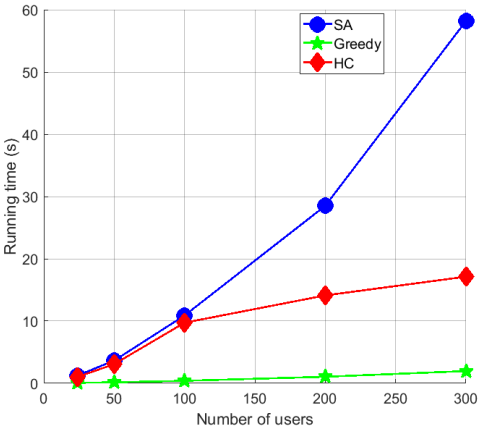

Fig. 9. Running time: comparison SA/HC/greedy [8] algorithms with two frequency carriers available.

An analysis with eight different frequency carriers was also carried out in Fig. 10 and Fig. 11. As in [8] the number of users allocated by the greedy algorithm does not increase after 100 users. The running time of SA is also reduced as there are more instances of frequency plans that comply with the interference requirements so the convergence is faster. Until 200 users, SA has similar performance and running time as the ILP algorithm proposed in [8]. ILP duration was limited to 60s, SA on the contrary converged even for 200 users in less than 40 s. ILP provides in [8] +33% users allocated compared to the greedy algorithm in the 200 users case, whereas SA provides here +88% users. HC performs similarly as SA in this case. With eight frequency carriers instead of previously two, the problem is less constrained and there exist several local optimum close to the global optimum.

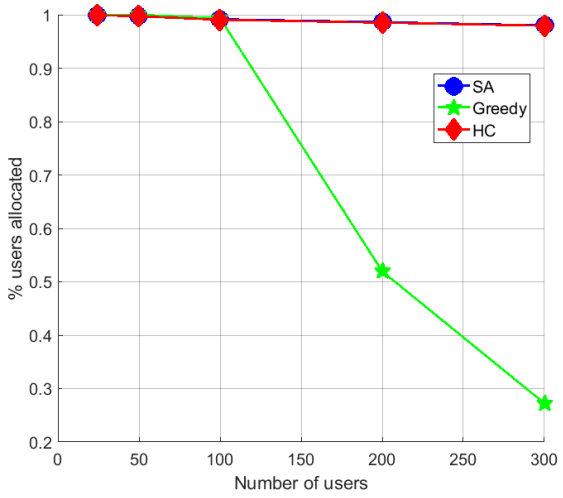

Fig. 10. Comparison SA/HC/greedy [8] algorithms with eight frequency carriers available.

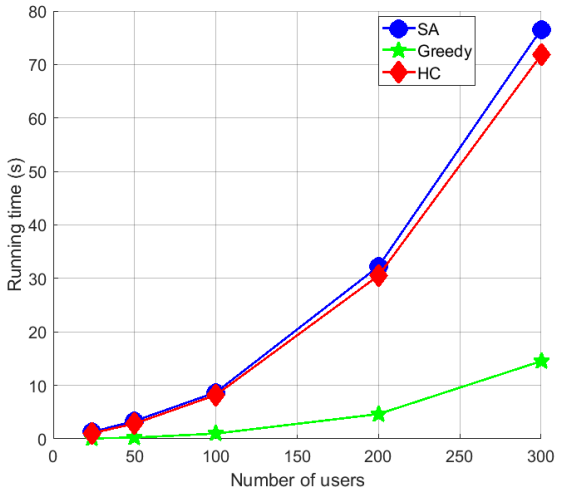

Fig. 11. Running time: comparison SA/HC/greedy [8] algorithms with eight frequency carriers available.

Allocation strategies can be implemented to limit the number of SA runs as it can reach a running time of 80 s for 300 users as presented in Fig. 9. As the satellite orbits and new users require data rate, the fast greedy algorithm can be used. SA can then be run only when the UTs are expected to be too much impacted by interference. The ground station are then required to anticipate the traffic 80 s before the arrival of the satellite to perform the optimisation.

V. Conclusion

To exploit the flexibility of advanced digital payload architecture and active antennas, efficient resource allocation algorithms must be implemented. With power, frequency and beamforming degrees of freedom, the algorithm proposed in this paper allows a fair spectral efficiency distribution. The frequency allocation algorithm based on simulated annealing prevents two close user beams to interfere between each other. Precoding reduces interference and the smart power allocation compensates for the scan and path losses by transferring power from the center to the edge of the coverage. Simulating annealing was identified as an efficient resource allocation algorithm compared to a greedy algorithm found in the literature with high allocation rate at the cost of higher running times. A hill climbing approach may offer a compromise between both optimisation techniques. The joint resource allocation may be an enabler for future spectral efficient satellite communication based on SDMA.

References

[1] H. Fenech *et al.*, "Future High Throughput Satellite systems," in *Proc. IEEE First AESS European Conference on Satellite Telecommunications (ESTEL)*, Rome, Italy, Oct., 2012.

[2] *NGMN 5G White Paper*, 2015.

[3] S. H. Blumenthal, "Medium Earth Orbit Ka band Satellite Communications System," in *Proc. IEEE Military Communications Conference*, 2013.

[4] S. Malloy, "NGSO Constellation – O3b, mPower," in *Proc. ITU Satellite Symposium*, 2019.

[5] R. H. Roy, "Spatial division multiple access technology and its application to wireless communication systems," in *Proc. IEEE 47th Vehicular Technology Conference. Technology in Motion*, 1997.

[6] E. Corbel, I. Buret, J.-D. Gayrard, G. E. Corazza and A. Bolea-Alamanac, "Hybrid satellite and terrestrial mobile network for 4G: Candidate architecture and space segment dimensioning.," in *Proc. ASMS*, 2008.

[7] R. De Gaudenzi, P. Angeletti, D. Petrolati and E. Re, "Future technologies for very high throughput satellite systems," *Int. J. Satellite Commun. Netw.*, Jul. 2019.

[8] L. Houssin, C. Artigues and E. Corbel, "Frequency allocation problem in a SDMA satellite communication system," in *Proc. 39th International Conference on Computers & Industrial Engineering (CIE39)*, Troyes, France, Jul., 2009, pp.1611-1616.

[9] K. Kiatmanaroj, C. Artigues, L.Houssin and E. Corbel, "Greedy algorithms for time-frequency allocation in a SDMA satellite communication system," in *Proc. 9th International Conference of Modeling, Optimization and Simulation*, Bordeaux, France, Jun., 2012.

[10] K. Kiatmanaroj, C. Artigues, L.Houssin and F. Messine, "Frequency allocation in a SDMA satellite communication system with beam moving," in *Proc. IEEE International Conference on Communications (ICC)*, Ottawa, Canada, Nov., 2012.

[11] J. Montesinos, "Traitement d'antenne SDMA pour système de télécommunications par satellite avec couverture dispersée," PhD. Dissertation, pp. 26, ISAE Supaero, Toulouse, France, 2009.

[12] G. Taricco, "Linear Precoding Methods for Multi-Beam Broadband Satellite Systems," in *Proc. 20th European Wireless Conf.*, May 2014, pp. 1-6.

[13] F. Vidal, H. Legay, G. Goussetis, A. Segneri, "On-board Precoding for Inter-beam Interference Mitigation applied to a Sparse Array for a MEO Satellite Broadband Application," submitted to *International Journal of Satellite Communication and Networking*, 2020.

[14] M. C. Vigano, G. Toso, G. Caille, C. Mangenot, I. E. Langer, "Sunflower Array Antenna with Adjustable Density Taper," International Journal of Antennas and Propagation, Apr. 2009.

[15] D. Tse and P. Viswanath, *Fundamentals of Wireless Communication*, 1st edition, Cambridge University Press, pp. 362, May 2005.
[16] S. D'Addio and V. Valenta, "Non-linearity assessment of sspa-based active antennas by means of a time-domain correlation method," in *Proc. 4th ESA Workshop on Advanced Flexible Telecom Payloads*, 2019.
[17] *Digital Video Broadcasting (DVB);Implementation guidelines for the second generation system for Broadcasting, Interactive Services, News Gathering and other broadband satellite applications; Part 1: DVB-S2*, ETSI TR 102 376-1 V1.2.1, pp. 94, table D.2: modulation and coding schemes and required Es/N0 considered in the simulations, 2015.
[18] SES, https://o3bmpower.ses.com, 2020.
[19] I. Khaled, A. El Falou, C. Langlais, B. El Hassan, M. Jezequel, "Non-linearity assessment of sspa-based active antennas by means of a time-domain correlation method," in *Proc. 4th ESA Workshop on Advanced Flexible Telecom Payloads*, 2019.
[20] P. Angeletti, R. De Gaudenzi, "A Pragmatic Approach to Massive MIMO for Broadband Communication Satellites," IEEE Access, vol. 8, 2020.
[21] G. Cocco, T. De Cola, M. Angelone and Z. Katona, "Radio Resource Management Strategies for DVB-S2 Systems Operated with Flexible Payloads," *8th Advanced Satellite Multimedia Systems Conference and the 14th Signal Processing for Space Communications Workshop*, 2016.
[22] H. Boche and M. Schubert, "Theoretical and experimental comparison of optimization criteria for downlink beamfoming," Europ. Trans. On Telecomm. (ETT), vol. 12, no. 5, pp. 417–426, Sept. 2001.
[23] *Digital Video Broadcasting (DVB): Second Generation Framing Structure, Channel Coding and Modulation Systems for Broadcasting, Interactive Services, News Gathering and Other broadband Satellite Applications: Part 2: DVB-S2 Extensions (DVB-S2X)*, document ETSI EN 302 307-2, 2014.
[24] F. Vidal et al., "A Methodology to Benchmark Flexible Payload Architectures in a Megaconstellation Use-case," *Int. J. Satellite Commun. Netw., Special Issue on Megaconstellations*, 2020. [Online]. Available: https://doi.org/10.1002/sat.1344
[25] *Terrestrial and space services sharing frequency bands above 1GHz*, ITU-R RR, Article 21, *International Telecommunications Union*, 2016.